



## COVID-19 Research Tools

Defeat the SARS-CoV-2 Variants

InvivoGen



### Dendritic Cells Regulate GPR34 through Mitogenic Signals and Undergo Apoptosis in Its Absence

This information is current as of February 26, 2022.

Elisabeth Jäger, Angela Schulz, Vera Lede, Chen-Ching Lin, Torsten Schöneberg and Diana Le Duc

*J Immunol* 2016; 196:2504-2513; Prepublished online 5 February 2016;

doi: 10.4049/jimmunol.1501326

<http://www.jimmunol.org/content/196/6/2504>

**Supplementary Material** <http://www.jimmunol.org/content/suppl/2016/02/04/jimmunol.1501326.DCSupplemental>

**References** This article **cites 46 articles**, 7 of which you can access for free at: <http://www.jimmunol.org/content/196/6/2504.full#ref-list-1>

**Why *The JI*?** [Submit online.](#)

- **Rapid Reviews! 30 days\*** from submission to initial decision
- **No Triage!** Every submission reviewed by practicing scientists
- **Fast Publication!** 4 weeks from acceptance to publication

*\*average*

**Subscription** Information about subscribing to *The Journal of Immunology* is online at: <http://jimmunol.org/subscription>

**Permissions** Submit copyright permission requests at: <http://www.aai.org/About/Publications/JI/copyright.html>

**Email Alerts** Receive free email-alerts when new articles cite this article. Sign up at: <http://jimmunol.org/alerts>



# Dendritic Cells Regulate GPR34 through Mitogenic Signals and Undergo Apoptosis in Its Absence

Elisabeth Jäger,<sup>\*,†</sup> Angela Schulz,<sup>\*,‡</sup> Vera Lede,<sup>\*</sup> Chen-Ching Lin,<sup>§</sup> Torsten Schöneberg,<sup>\*</sup> and Diana Le Duc<sup>\*</sup>

Dendritic cells (DCs) are specifically equipped with the G protein–coupled receptor 34 (GPR34). Tight regulation of GPR34 gene expression seems highly important for proper immunological functions, because the absence of this receptor leads to an alteration of the immune response, whereas overexpression was reported to be involved in neuroinflammation. However, the regulatory mechanism of GPR34 expression has not yet been investigated. Whole-transcriptome RNA sequencing analysis from spleens and DCs of GPR34 knockout and wild-type mice, combined with protein–protein interaction data, revealed functional modules affected by the absence of this receptor. Among these, NF- $\kappa$ B, MAPK, and apoptosis-signaling pathways showed high significance. Using murine DCs we experimentally show that NF- $\kappa$ B and MAPK pathways are involved in the downregulation of GPR34. DCs lacking GPR34 have a higher caspase-3/7 activity and increased apoptosis levels. Our study reveals a novel role of GPR34 in the fate of DCs and identifies a regulatory mechanism that could be relevant for treatment of GPR34-overexpressing pathologies, such as neuroinflammatory or cancer conditions. *The Journal of Immunology*, 2016, 196: 2504–2513.

Dendritic cells (DCs) are essential for the initiation of a proper immune response, and they are considered the sentinels of the immune system, given their ability to sample the microenvironment, process, and present the Ags to the naive T cells (1). P2Y purinergic receptors are expressed and regulated in a stage-specific manner during the differentiation of DCs from blood precursor cells (2). These receptors have been suggested to play an important role in the maturation of DCs (2), a crucial requirement for an adequate immune response (3).

The G protein–coupled receptor 34 (GPR34) belongs to the P2Y<sub>12</sub>-like receptor subgroup of the rhodopsin class. GPR34 was first described after mining GenBank for novel G protein–coupled receptor (GPCR) sequences and was assigned to the human X chromosome (4). Although lysophosphatidylserine was proposed as a potential endogenous ligand (5), subsequent studies found no

support that this is the natural ligand but rather a surrogate agonist (6, 7). Hence, GPR34 is still classified as an orphan in the International Union of Basic and Clinical Pharmacology database (8).

GPR34 is highly expressed in immune cells (macrophages and microglia) (6, 9) and immune system–derived cell lines (HL-60, K562, WEHI-3B, RAW 264.7, P815) (10). Immune system–challenging conditions on mice showed that GPR34 deficiency results in an improper immune response, with higher susceptibility to systemic infections (6). This is most probably due to altered phagocytosis in GPR34-deficient mice (11). Despite clear identification of the transcriptional starts in both the rodent and human GPR34 genes, in vitro attempts to identify the promoter and characterize its regulation were unsuccessful (10). Nevertheless, up-regulation of this GPCR was reported in activated microglia after treatment with a demyelinating toxin, suggesting an involvement of GPR34 in neuroinflammation (9). These findings indicate that the regulation of GPR34 is important for adequate immune functions.

In this study, we aimed to understand how DC stimulation impacts the regulation of an immune-related receptor, GPR34. Using a combination of RNA sequencing (RNA-Seq) analyses and functional studies in immune cells derived from wild-type (WT) and GPR34 knockout (KO) mice, we found that MAPK and NF- $\kappa$ B signaling tightly control GPR34 expression. GPR34-deficient DCs show a commitment to apoptosis, which could result in the altered immune response described in this KO mouse (6).

## Materials and Methods

Unless stated otherwise, all standard substances were purchased from Sigma-Aldrich (Taufkirchen, Germany), Merck (Darmstadt, Germany), and Carl Roth (Karlsruhe, Germany). R-848 and LPS were obtained from Enzo Life Sciences (Lörrach, Germany). PMA was purchased from Tocris Bioscience (Bristol, U.K.). Celastrol and U0126 were supplied by Cayman Chemicals (Ann Arbor, MI) and Sigma-Aldrich. Cell culture material was obtained from Sarstedt (Nümbrecht, Germany), and primers were purchased from Invitrogen (Eggenstein, Germany).

## Animals

Animals were maintained in a controlled animal facility with 21°C room temperature, 55% humidity, and a 12/12-h light/dark cycle. All animal experiments were conducted in accordance with accepted standards of

<sup>\*</sup>Institute of Biochemistry, University of Leipzig, 04103 Leipzig, Germany; <sup>†</sup>Rheumatology Unit, Department of Internal Medicine, University of Leipzig, 04103 Leipzig, Germany; <sup>‡</sup>Integrated Research and Treatment Center Adiposity Diseases, Medical Faculty, University of Leipzig, 04103 Leipzig, Germany; and <sup>§</sup>Institute of Biomedical Informatics, National Yang-Ming University, Taipei 11221, Taiwan

ORCID: 0000-0003-2336-1573 (A.S.); 0000-0001-7289-2552 (D.L.D.).

Received for publication June 12, 2015. Accepted for publication January 3, 2016.

This work was supported by intramural support from the Medical Faculty, University of Leipzig, the Bundesministerium für Bildung, Wissenschaft, Forschung und Technologie (Integrated Research and Treatment Center Adiposity Diseases Leipzig), and Deutsche Forschungsgemeinschaft Grant FOR748.

RNA sequencing reads and expression profiles have been submitted to the Gene Expression Omnibus (<http://www.ncbi.nlm.nih.gov/geo/>) under accession number GSE68155.

Address correspondence and reprint requests to Dr. Torsten Schöneberg and Dr. Diana Le Duc, Institute of Biochemistry, Molecular Biochemistry, Medical Faculty, University of Leipzig, Johannisallee 30, 04103 Leipzig, Germany. E-mail addresses: schoberg@medizin.uni-leipzig.de (T.S.) and diana\_leduc@eva.mpg.de (D.L.D.).

The online version of this article contains supplemental material.

Abbreviations used in this article: DC, dendritic cell; GO, Gene Ontology; GPCR, G protein–coupled receptor; GPR34, G protein–coupled receptor 34; KO, knockout; PARP, poly(ADP-ribose) polymerase; RNA-Seq, RNA sequencing; WT, wild-type.

Copyright © 2016 by The American Association of Immunologists, Inc. 0022-1767/16/\$30.00

humane animal care and approved by the respective regional government agencies of Saxony (T07/13, A17/12).

The generation and initial characterization of the GPR34-deficient mouse strain were previously reported (6). KO mice were backcrossed for >12 generations onto the C57BL/6J background. Subsequently, every fifth generation of WT and KO mice was intercrossed to avoid background differences.

### Primary cell cultures and cell stimulation

For DC cultures, bone marrow was isolated from femurs and tibiae of 8- to 16-wk-old male WT or KO mice as previously described (12, 13). Cells ( $4 \times 10^6$ ) were plated and further cultivated for 10 d at 37°C in a humidified atmosphere containing 5% CO<sub>2</sub> in a 3:2 mixture of RPMI 1640 supplemented with 10% heat-inactivated FBS, 2 mM L-glutamine, 100 U/ml penicillin, 100 µg/ml streptomycin, 50 µM 2-ME, and a supernatant from a GM-CSF-secreting X63 cell line.

DCs were harvested on day 10 and seeded ( $3 \times 10^6$  cells in 2.5 ml serum-free RPMI 1640) in 6-cm dishes. On day 11, DCs were preincubated with the indicated inhibitors for 30 min and subsequently incubated with the different TLR stimulants or MAPK/NF-κB activators for 8 h. At the end of incubation time, cells were harvested in 500 µl TRI Reagent (Sigma-Aldrich) following RNA isolation, reverse transcription, and RT-PCR or library preparation.

For splenocytes cultures, spleens were collected from 8- to 16-wk-old male WT mice. Furthermore, they were cut in smaller pieces and disintegrated in 5 ml PBS through a 70-µm cell strainer. After sedimentation of the splenocytes, the pellet was resuspended in 1 ml erythrocyte lysing buffer. After 2 min the cell suspension was centrifuged and washed twice with PBS. Cells ( $5 \times 10^6$ ) were seeded in 24-well plates in 500 µl splenocyte medium (RPMI 1640 with 10% FBS, 2 mM L-glutamine, 100 U/ml penicillin, and 100 µg/ml streptomycin). The cells were incubated with LPS (5 µg/ml) for 8 h at 37°C and 5% CO<sub>2</sub>. After the incubation time cells were harvested in TRI Reagent following RNA isolation and RT-PCR.

Microglia cells were prepared from brains of 3- to 5-d-old WT and KO mice. Briefly, meninges were mechanically removed and cells were cultured in DMEM (Invitrogen) supplemented with 10% FBS, 100 U/ml penicillin, and 100 µg/ml streptomycin at 37°C in a humidified 5% CO<sub>2</sub> incubator. After reaching confluency, cocultures were stimulated with medium supplemented with M-CSF from L929 fibroblasts. Microglia cells were detached from the microglia-astrocyte cocultures by shaking and seeded in a six-well plate ( $4 \times 10^5$  cells/well). Next day, attached microglia cells were treated for 8 h with LPS (5 µg/ml) and cells were harvested in TRI Reagent following RNA isolation and RT-PCR.

### RNA-Seq analysis

For library preparation and sequencing, total RNA was extracted from DC cultures and spleen samples using the TRI Reagent according to the manufacturer's instructions. The quality and quantity of the purified RNA were determined by measuring the absorbance at 260/280 nm ( $A_{260}/A_{280}$ ) using a NanoDrop spectrophotometer. Indexed cDNA libraries with an average insert size of 300 bp were constructed using the TruSeq RNA sample preparation kits v2 (Illumina, San Diego, CA). Spleen libraries from WT ( $n = 10$ ) and KO ( $n = 9$ ) were pooled and loaded onto two flow cell channels. DC cultures libraries were performed in three biological replicates for each group: KO, WT, unstimulated, and LPS stimulated, respectively. A minimum of 7.9 million reads per library were sequenced.

### Transcriptome analysis

After assigning reads to samples according to library index, we used a sequencing pipeline to trim the adapters and remove reads <60 bp (14). Reads were mapped to the mouse genome July 2007 NCBI37/mm9 with Ensembl v66 annotations (15) using TopHat 1.3.3 (16). We excluded reads that mapped to the mitochondrial genome and reads that did not map uniquely to the reference nuclear genome. The transcription level for each gene was obtained by intersecting mapping results with gene annotations using BEDTools (17). We used the DESeq package in R (18) to determine differentially expressed genes. The package uses a negative binomial fit and corrects for multiple testing using the Benjamini-Hochberg procedure.

### Identification of functional modules in KO

To identify the functional modules related to GPR34 deficiency, we used the RNA-Seq data from the two spleen experimental groups: 1) WT and 2) KO. We further integrated expression profiles with protein-protein interactions to identify the condition-specific functional modules in these four experimental groups (19). The functional modules identified were termed as FM<sub>1</sub> (WT) and FM<sub>2</sub> (KO). We inferred the set of putative functional modules in the KO (FM<sub>KO</sub>) as  $FM_{KO} = FM_2 - FM_1$ , where the operator “−” calculates the difference of two sets, that is, FM<sub>2</sub> − FM<sub>1</sub> refers to the functional modules in FM<sub>2</sub> but not in FM<sub>1</sub>. Accordingly, FM<sub>KO</sub> contained the functional modules activated in GPR34-deficient mice, but not in WT mice.

### Gene Ontology pathways analysis

To identify metabolic pathways disrupted in DCs as a consequence of GPR34 absence we tested for functional enrichment in Gene Ontology (GO) categories (20) using the hypergeometric test implemented in FUNC (21). An

Table I. The top 20 significantly enriched functional modules in KO mice

Functional Module	Module Size		Significance	
	No. Nodes	No. Edges	$P_{con}$	$P_{net}$
Ag receptor-mediated signaling pathway <sup>a</sup>	52	33	$4.17 \times 10^{-13}$	$4.70 \times 10^{-9}$
Regulation of I-κB kinase/NF-κB signaling <sup>b</sup>	111	70	$3.93 \times 10^{-9}$	$4.77 \times 10^{-8}$
Immune response-regulating cell surface receptor signaling pathway <sup>a</sup>	58	35	$8.46 \times 10^{-10}$	$1.10 \times 10^{-7}$
Positive regulation of I-κB kinase/NF-κB signaling <sup>b</sup>	81	49	$7.65 \times 10^{-6}$	$1.18 \times 10^{-6}$
Regulation of IL-2 production <sup>a</sup>	28	12	$8.21 \times 10^{-4}$	$9.19 \times 10^{-6}$
Positive regulation of IL-2 production <sup>a</sup>	19	9	$2.19 \times 10^{-3}$	$1.50 \times 10^{-5}$
Regulation of actin filament polymerization	52	19	$1.07 \times 10^{-4}$	$1.56 \times 10^{-5}$
Regulation of protein polymerization	63	22	$4.23 \times 10^{-5}$	$2.53 \times 10^{-5}$
Ag processing and presentation of exogenous peptide Ag via MHC class II <sup>a</sup>	10	6	$3.32 \times 10^{-3}$	$3.02 \times 10^{-5}$
TCR signaling pathway <sup>a</sup>	31	13	$4.25 \times 10^{-8}$	$3.85 \times 10^{-5}$
Regulation of actin polymerization or depolymerization	55	19	$1.67 \times 10^{-3}$	$7.76 \times 10^{-5}$
Regulation of cellular catabolic process	348	144	$1.51 \times 10^{-10}$	$1.11 \times 10^{-4}$
Regulation of stress-activated MAPK cascade <sup>c</sup>	91	38	$1.08 \times 10^{-7}$	$1.31 \times 10^{-4}$
Regulation of stress-activated protein kinase signaling cascade <sup>c</sup>	92	38	$6.96 \times 10^{-8}$	$1.52 \times 10^{-4}$
Regulation of nucleocytoplasmic transport	99	28	$6.08 \times 10^{-9}$	$1.57 \times 10^{-4}$
Negative regulation of programmed cell death <sup>d</sup>	332	199	$1.29 \times 10^{-14}$	$2.31 \times 10^{-4}$
Modification-dependent macromolecule catabolic process	191	98	$2.40 \times 10^{-22}$	$3.63 \times 10^{-4}$
Regulation of protein transport	175	57	$3.01 \times 10^{-8}$	$4.10 \times 10^{-4}$
Negative regulation of organelle organization	113	27	$1.11 \times 10^{-7}$	$4.10 \times 10^{-4}$

These selected top 20 functional modules were ranked by  $P_{net}$ .

<sup>a</sup>Functions related to Ig-mediated response.

<sup>b</sup>Functions related to I-κB kinase/NF-κB signaling.

<sup>c</sup>Functions related to regulation of stress-activated MAPK cascade.

<sup>d</sup>Functions related to regulation of cell death.

No. Edges, number of coexpressed protein-protein interactions involved in the corresponding functional module; No. Nodes, number of proteins involved in the corresponding functional module;  $P_{con}$ ,  $p$  value derived from the conventional functional enrichment analysis, which only considers the amount of protein in a module;  $P_{nets}$ ,  $p$  value derived from our integrative network analysis, which considers the enrichment of coexpressed protein-protein interactions in a module.

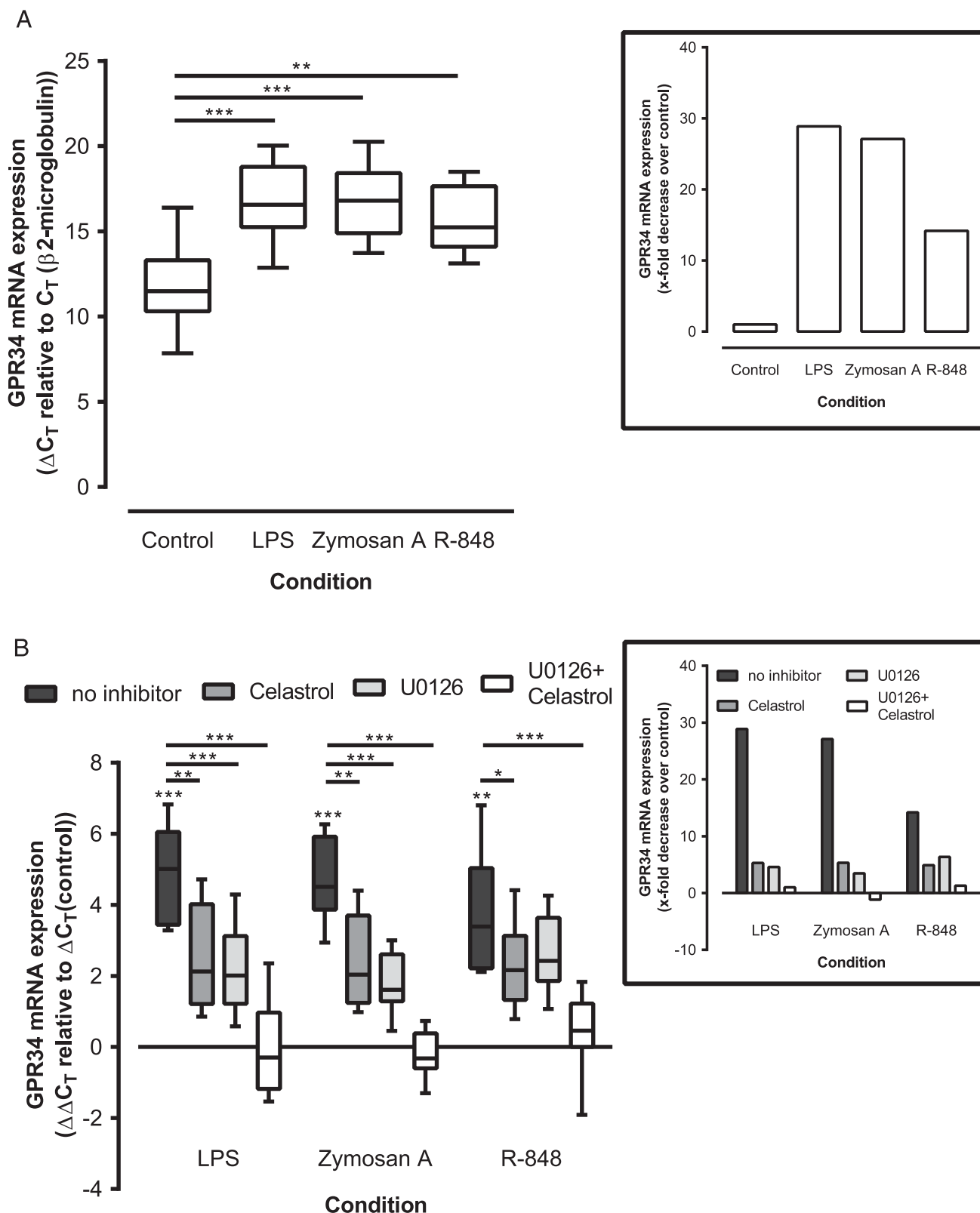
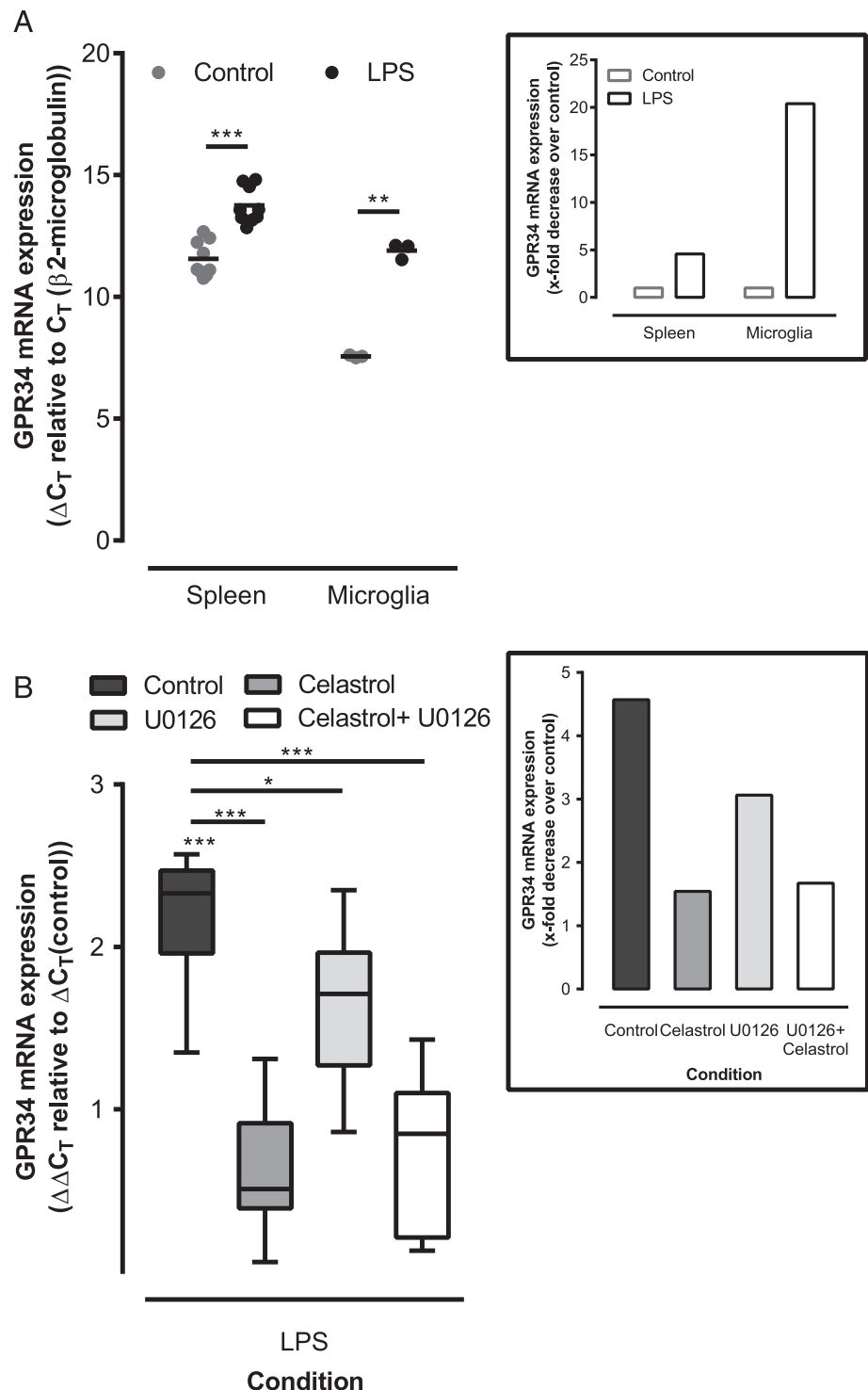


**FIGURE 1.** GPR34 mRNA levels in murine cultured DCs are decreased by TLR stimulation. **(A)** Bone marrow-derived DCs were incubated for 8 h with different compounds (details in *Materials and Methods*) or they were left unstimulated (Control) and GPR34 mRNA levels were quantified by RT-PCR. Several TLR agonists (LPS, zymosan A, and R-848) significantly decreased GPR34 mRNA levels. Data are presented as GPR34 mRNA level  $\Delta C_T$  difference to  $\beta 2$ -microglobulin;  $n = 9$  independent experiments (biological replicates) performed in duplicates. **(B)** MEK/ERK1/2 and NF- $\kappa$ B inhibitors significantly inhibited the decreasing effect TLR agonists have on GPR34 mRNA levels. Data are presented as GPR34 mRNA level  $\Delta \Delta C_T$  difference to control (RPMI 1640 medium,  $\Delta C_T = 11.95$ ) as box-and-whisker plots of  $n = 9, 8, 7$ , and  $8$  (no inhibitor, celestrol, U0126, and celestrol plus U0126) independent experiments (biological replicates) performed in duplicates. Center lines show the medians; box limits indicate the 25th and 75th percentiles as determined by GraphPad Prism software; whiskers extend to minimum and maximum values. Corresponding figure *insets* show the fold change of mRNA levels decrease calculated as  $2^{\text{average } \Delta \Delta C_T}$ .  $*p < 0.05$ ,  $**p < 0.01$ ,  $***p < 0.001$ .

**FIGURE 2.** GPR34 mRNA levels are decreased after LPS stimulation. **(A)** Splenocytes and microglia were incubated for 8 h with LPS or left unstimulated (Control) (details in *Materials and Methods*) and GPR34 mRNA levels were quantified by RT-PCR. Data are presented as GPR34 mRNA level  $\Delta C_T$  difference to  $\beta_2$ -microglobulin;  $n_{\text{spleen}} = 9$  and  $n_{\text{microglia}} = 3$  independent experiments (biological replicates) performed in duplicates. **(B)** For splenocytes, the mRNA decreasing effect of TLR4 stimulation could be repressed through MAPK and NF- $\kappa$ B inhibitors. Data are presented as GPR34 mRNA level  $\Delta\Delta C_T$  difference to control (RPMI 1640 medium,  $\Delta C_T = 11.56 \pm 0.73$ ) as box-and-whisker plots of  $n = 9, 9, 9$ , and 7 (no inhibitor, celestrol, U0126, and celestrol plus U0126) independent experiments (biological replicates) performed in duplicates. Center lines show the medians; box limits indicate the 25th and 75th percentiles as determined by GraphPad Prism software; whiskers extend to minimum and maximum values. Corresponding figure insets show the fold change of mRNA levels decrease calculated as  $2^{\text{average } \Delta\Delta C_T}$ . \* $p < 0.05$ , \*\* $p < 0.01$ , \*\*\* $p < 0.001$ .



adjusted  $p$  value (Benjamini–Hochberg) of  $<0.05$  was used as significance threshold. By separately analyzing gene expression from unstimulated and LPS-stimulated WT and KO originating DCs, we could differentiate between pathway disruption in the basal and activation state, respectively.

RNA-Seq reads and expression profiles have been deposited in Gene Expression Omnibus (<http://www.ncbi.nlm.nih.gov/geo/>) under project ID GSE68155.

#### TLR stimulation and downstream pathways assessment

On day 11, DCs were incubated with different compounds for 8 h: LPS (5  $\mu\text{g/ml}$ ), zymosan A (50  $\mu\text{g/ml}$ ),  $\text{MnCl}_2$  (300  $\mu\text{M}$ ), R-848 (1  $\mu\text{g/ml}$ ), and PMA (500 ng/ml). To inhibit NF- $\kappa$ B and/or MAPK pathways, DCs were preincubated for 30 min with celestrol (NF- $\kappa$ B inhibitor; 500 nM) and/or U0126 (MEK/ERK 1/2 inhibitor; 50  $\mu\text{M}$ ).

The specificity of the substances under the employed conditions was confirmed using AlphaScreen (PerkinElmer) assays and Western blots. Cytotoxicity effects were tested using the Cell Counting Kit-8 (Dojindo Molecular Technologies) and a neutral red assay (22) (in the case of  $\text{MnCl}_2$ ). The used stimulants/inhibitors proved high specificity and non-significant cytotoxic effects, which allowed their use in experiments.

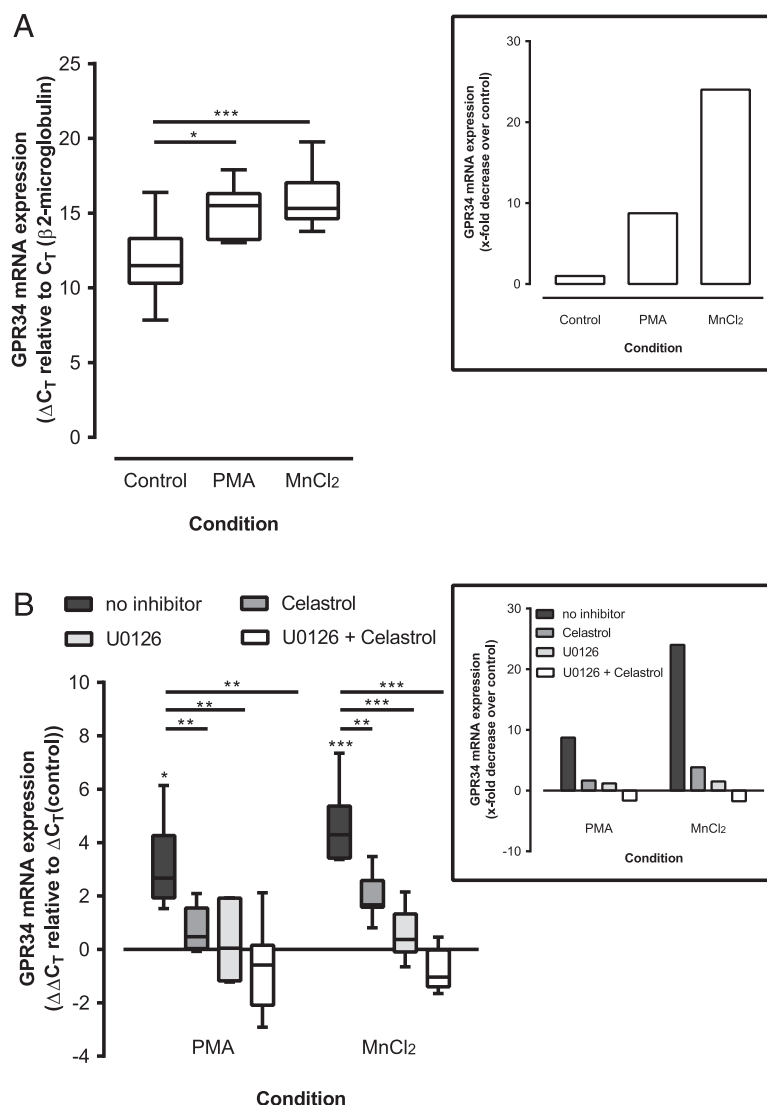
After preincubation with the inhibitors, the test substance was added onto DCs (12). At the end of the incubation time, cells were harvested in 500  $\mu\text{l}$  TRI Reagent following RNA isolation and RT-PCR.

The effect of LPS on GPR34 regulation was additionally tested on microglia and splenocytes after 8 h stimulation at a concentration of 5  $\mu\text{g/ml}$ .

For the pulse kinetic analysis of GPR34, DCs were incubated for 1 h with LPS (5  $\mu\text{g/ml}$ ). Afterwards, the LPS-containing medium was replaced with RPMI 1640 medium and cells were harvested in 500  $\mu\text{l}$  TRI Reagent at 1, 2, 4, 8, 16, and 24 h following RNA isolation and RT-PCR.



**FIGURE 3.** GPR34 mRNA levels in murine cultured DCs are significantly reduced after direct stimulation of MAPK and NF- $\kappa$ B. **(A)** Bone marrow-derived DCs were incubated for 8 h with PMA, MnCl<sub>2</sub>, or left unstimulated (Control) (details in *Materials and Methods*) and GPR34 mRNA levels were quantified by RT-PCR. Data are presented as GPR34 mRNA level  $\Delta C_T$  difference to  $\beta_2$ -microglobulin;  $n = 9$  independent experiments (biological replicates) performed in duplicates. **(B)** MEK/ERK1/2 and NF- $\kappa$ B inhibitors significantly inhibited the decreasing effect that either PMA or MnCl<sub>2</sub> have on GPR34 mRNA level. Data are presented as GPR34 mRNA level  $\Delta\Delta C_T$  difference to control (RPMI 1640 medium,  $\Delta C_T = 11.95$ ) as box-and-whisker plots of  $n = 9, 8, 7$ , and 8 (no inhibitor, celastrol, U0126, celastrol plus U0126) independent experiments (biological replicates) performed in duplicates. Center lines show the medians; box limits indicate the 25th and 75th percentiles as determined by GraphPad Prism software; whiskers extend to minimum and maximum values. Corresponding figure insets show the fold change of mRNA levels decrease calculated as  $2^{\text{average } \Delta\Delta C_T}$ . \* $p < 0.05$ , \*\* $p < 0.01$ , \*\*\* $p < 0.001$ .



#### cDNA preparation and quantification by RT-PCR

Total RNA was isolated from cultured DCs using TRI Reagent according to the manufacturer's instructions. RNA (550 ng) was reverse transcribed (SuperScript, Invitrogen) with oligo(dT) primer in a total reaction volume of 20  $\mu$ l. cDNA (1  $\mu$ l) was further subjected to RT-PCR using Platinum SYBR Green RT-PCR Supermix (Invitrogen), forward and reverse primers (0.9  $\mu$ M), and 5-carboxy-X-rhodamine (passive reference dye) (100 nM). Primers for *Gpr34* were designed with the Primer3 software corresponding to Exon 2 (sense primer, 5'-GCTTCTGAAGTATGGCCTGAA-3') and Exon 3 (antisense primer, 5'-TTCCATGAGAGGAGCAAAGC-3') of the *Gpr34* mouse gene.  $\beta_2$ -Microglobulin was measured as housekeeping gene (sense primer, 5'-GCTATCCAGAAAACCCCTCAAA-3', antisense primer, 5'-GGCGGGTGAAGTGTGTTA-3'). PCR was performed in an Mx3000P instrument (Stratagene, La Jolla, CA) using the following protocol: 5 min at 50°C, 2 min at 95°C, and 40 cycles of 15 s at 95°C, 30 s at 60°C. A product melting curve confirmed the presence of a single amplicon. The correct amplicon size was checked by agarose gel electrophoresis. Cycle threshold ( $C_T$ ) values were set within the exponential phase of the PCR. After normalization to  $\beta_2$ -microglobulin,  $\Delta C_T$  ( $C_T$  (GPR34) -  $C_T$  ( $\beta_2$ -MG)) values were used to calculate the relative expression levels ( $\Delta\Delta C_T$ ). Gene regulation was statistically evaluated by subjecting the  $\Delta\Delta C_T$  values to a two-sided, nonparametric Mann-Whitney test, assuming nonequal variances. Fold change of gene regulation is given as  $2^{\Delta\Delta C_T}$  values.

#### Caspase-3, poly(ADP-ribose) polymerase-1, ERK1/2, and I $\kappa$ B analyses

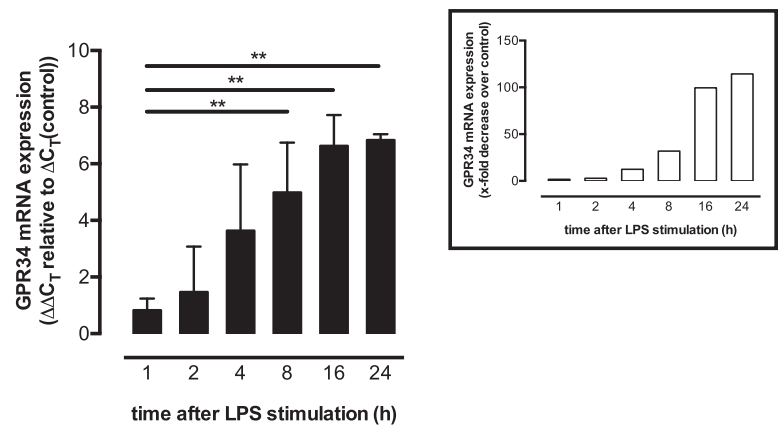
Caspase-3/7 activity was measured in 96-well plates using Caspase-Glo 3/7 assay (Promega, Madison, WI) according to the manufacturer's instruc-

tions. Briefly, bone marrow-derived DCs originating from four WT and KO mice each were seeded in white-walled 96-well plates at a density of 15,000 cells/well and kept in 50  $\mu$ l serum-free RPMI 1640 overnight. To detect caspase-3, activation cells were incubated with staurosporine (5  $\mu$ M; MP Biomedicals, Solon, OH) for 8 h. At the end of the incubation time the proluminescent substrate was added following the protocol instructions. Luminescence was determined using a PerkinElmer Life Sciences Wallac 1420 Victor<sup>2</sup> multilabel plate reader in luminescence mode and measurement time of 1 s.

To test whether caspase-3/7 activity was influenced by staurosporine and/or genotype (WT or KO mice) we used a linear mixed model (23) into which we included these two predictors as fixed effects and assay batch as random effect. The model was fitted in R (24) using the function lmer of the R package lme4 (25). The significance of the full model as compared with the null model (comprising only the random effects from the assay batch) was established using a likelihood ratio test (R function ANOVA with argument test set to Chisq). To achieve more reliable  $p$  values we fitted the models using maximum likelihood (23).

Western blots were performed to measure caspase-3 and poly(ADP-ribose) polymerase (PARP)-1 cleavage. Following incubation with staurosporine for 8 h, 3 million cells were lysed in RIPA lysis buffer containing a complete proteinase inhibitor mixture (Roche). The lysates were sonicated and the protein concentration was determined via a DC protein assay (Bio-Rad). Lysates were mixed with reducing Laemmli buffer and heated to 95°C for 5 min. Twenty to 30  $\mu$ g protein was loaded onto a 4–15% Mini-Protean TGX precast protein gel (Bio-Rad) or onto a large 10% polyacrylamide gel. Proteins were blotted to a nitrocellulose membrane (GE Healthcare) and cleaved caspase-3 (Cell Signaling Technology) or cleaved PARP-1 (GeneTex) was detected with specific Abs.

**FIGURE 4.** GPR34 mRNA levels are reduced after a pulse stimulation with LPS. Bone marrow–derived DCs were incubated for 1 h with LPS or RPMI 1640 (details in *Materials and Methods*) and GPR34 mRNA levels were quantified at subsequent time points by RT-PCR. Data are presented as GPR34 mRNA level  $\Delta\Delta C_T$  difference to control (same time point, RPMI 1640 medium) of  $n = 6, 3, 6, 6$ , and  $2$  (at 2, 4, 8, 16, and 24 h after LPS stimulation) independent experiments (biological replicates) performed in duplicates. The figure *inset* shows the fold change of mRNA levels decrease calculated as  $2^{\text{average } \Delta\Delta C_T}$ .  $**p < 0.01$ .



To measure ERK1/2 (p42/44) and I $\kappa$ B $\alpha$  phosphorylation 3 million DCs originating from three WT and KO mice each were stimulated for 30 min with 6  $\mu$ g/ml LPS. After performing the steps described above (except the sonication), lysates were loaded onto a 12% Mini-Protein TGX precast protein gel. The phosphorylated proteins were detected with specific Abs from Cell Signaling Technology.

Densitometry analyses of Western blot bands were performed with ImageJ. Band densities were normalized to the GAPDH band density. Phosphorylation levels in KO were calculated as percentage of WT and results were subjected to a Fisher exact test, using the fisher.test function in R (22).

#### Flow cytometry analysis of DCs

DCs were cultured for 10 d. To check the purity of the DC population, cells were labeled with CD11b and CD11c Abs. WT DC cultures consist of  $70.9 \pm 2.1\%$  and KO DC cultures are composed of  $77.1 \pm 3.8\%$  CD11b $^+$ /CD11c $^+$  cells (Supplemental Fig. 1,  $n = 4$  biological replicates,  $p < 0.05$ ). To check the percentage of apoptotic cells in KO and WT DC cultures, DCs were collected, washed with ice-cold PBS, and then resuspended in  $1 \times$  binding buffer at a concentration of  $1 \times 10^6$  cells/ml. Naive and staurosporine-treated DCs were stained with annexin V–allophycocyanin and propidium iodide for  $<30$  min according to the manufacturer's protocol (BD Biosciences). Annexin V $^+$ /propidium iodide $^-$  cells marked early apoptotic cells, whereas annexin V $^+$ /propidium iodide $^+$  cells indicated late apoptotic/dead cells. Cells were analyzed using the LSR II flow cytometer (BD Biosciences). The PerCP-Cy5.5–A channel shows propidium iodide staining; the laser excitation wavelength was 488 nm with 695/40 nm filter

sets to detect emission. Annexin V staining (allophycocyanin–A channel) was detected by 660/20 nm filters after laser excitation wavelength of 633 nm. Approximately 10,000 cells per sample were quantified using BD FACSDiva 8.0.1 (BD Biosciences). Unstained and single-stained cells were used to establish background fluorescence and to set quadrants before calculating the percentage of positive cells. The percentage of positive cells was calculated using simple ratios.

## Results

### Identification of GPR34-related functional modules

GPR34 deficiency leads to an impaired immune response only under challenging conditions (6). To understand the function of GPR34 more comprehensively, we conducted RNA-Seq analyses on spleens of KO and WT mice. Gene expression analysis detected 44 differentially expressed genes in KO mice, after multiple testing corrections (adjusted  $p < 0.1$ , data deposited in <http://www.ncbi.nlm.nih.gov/geo/> under accession no. GSE68155). Previous studies have shown that the integration of protein interaction network data with transcriptome information can facilitate a better understanding of the disease mechanism and its outcome (19, 26). To identify the functional modules putatively affected by GPR34 we thus integrated gene expression profiles with protein

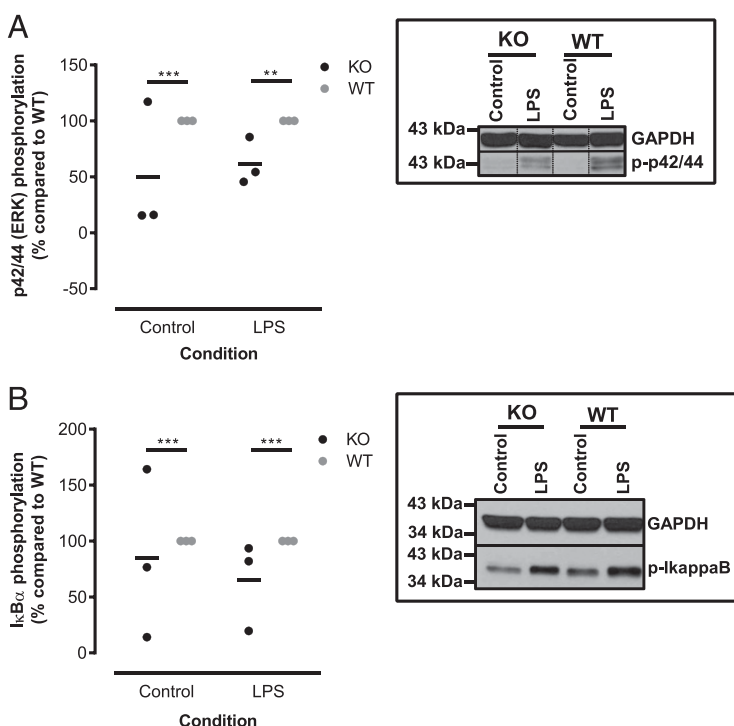
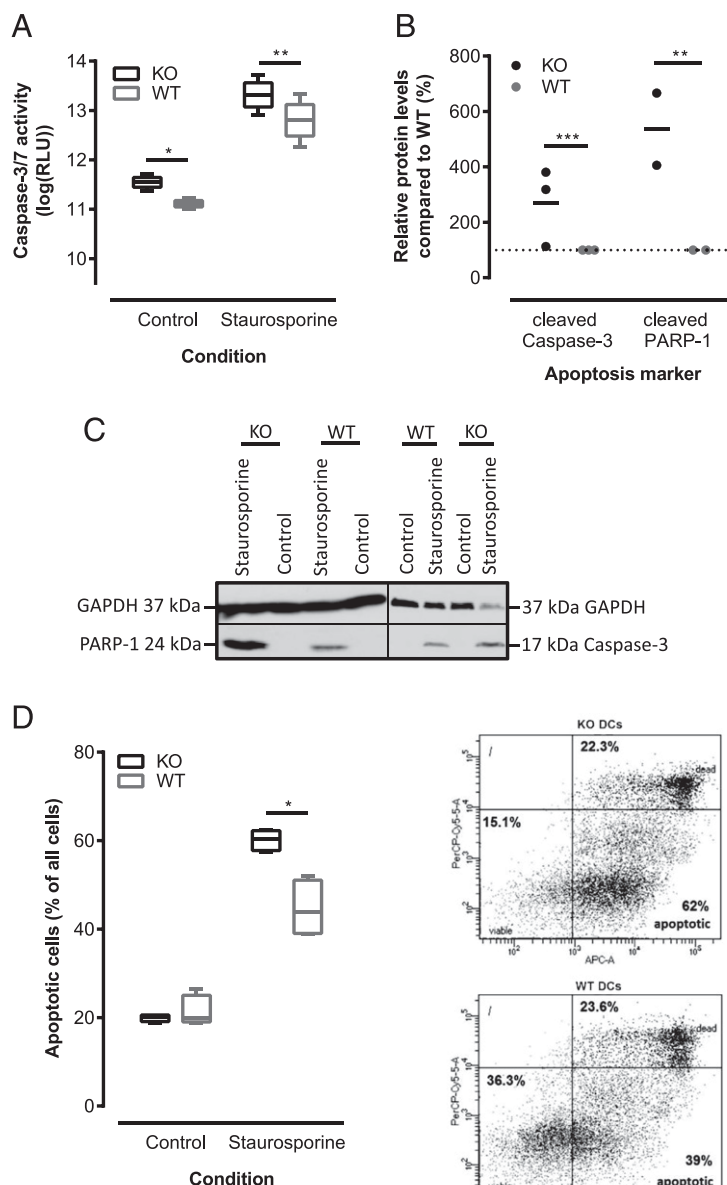


**FIGURE 5.** Absence of GPR34 results in increased ERK1/2 and I $\kappa$ B phosphorylation. Bone marrow–derived DCs were incubated for 30 min with LPS or RPMI 1640 (details in *Materials and Methods*) and (A) ERK1/2 and (B) I $\kappa$ B phosphorylation events were detected by Western blot analyses (details in *Materials and Methods*). Band intensities were measured on the Western blot images using ImageJ. Quantitation was performed after band intensity normalization to GAPDH, and KO (black) values are presented in the graph as percentage from the respective WT (gray) sample ( $n = 3$  KO, WT biological replicates). Horizontal lines show the mean. Statistical significance was tested using a Fisher exact test. The *inset* shows a representative Western blot gel image.  $**p < 0.01$ ,  $***p < 0.001$ .

**FIGURE 6.** GPR34 deficiency leads to increased apoptosis. **(A)** Caspase-3/7 activity was measured on DC cultures from KO (black) and WT (gray) mice. DCs were either under basal conditions or stimulated with staurosporine. A linear mixed model was used to test the effect of genotype and stimulant. The significance for staurosporine was tested using the likelihood ratio test comparing the model, including the genotype to the one with the random batch effect. Plot of  $n = 4$  (KO, WT) independent experiments (biological replicates) performed as two KO and two WT samples per batch. RLU, relative luminescence unit. **(B)** Staurosporine-induced caspase-3 and PARP-1 cleavages were detected by Western blot analyses. Quantitation was performed after band intensity normalization to GAPDH and KO (black) values are presented in the graph as percentage from the respective WT (gray) sample ( $n_{\text{caspase-3}} = 4$  and  $n_{\text{PARP-1}} = 2$  KO, WT biological replicates). Horizontal lines show the mean. Statistical significance was tested using a Fisher exact test. **(C)** Representative Western blot gel image of caspase-3 and PARP-1 cleavage in WT and KO DCs after staurosporine treatment. **(D)** The percentage of apoptotic cells in DC cultures after staurosporine treatment was quantified in DC cultures from KO (black) and WT (gray). Cells were stained with annexin V and propidium iodide. Annexin V<sup>+</sup>/propidium iodide<sup>-</sup> cells reflected early apoptotic cells, whereas annexin V<sup>+</sup>/propidium iodide<sup>+</sup> cells indicated late apoptotic/dead cells. The percentage of positive cells was calculated using simple ratios (details in *Materials and Methods*);  $n = 4$  (KO) and 5 (WT) independent experiments (biological replicates). Data are presented as box-and-whisker plots; center lines show the medians; box limits indicate the 25th and 75th percentiles as determined by GraphPad Prism software; whiskers extend to minimum and maximum values;  $n = 4$  (10,000 cells/sample). The *inset* shows one representative measurement. \* $p < 0.05$ , \*\* $p < 0.01$ , \*\*\* $p < 0.001$ .



interaction networks and constructed coexpressed protein interaction networks, which are the auxiliary networks to reveal condition-specific networks (details in *Materials and Methods*). By applying this analysis (19) to the spleen transcriptome data, originating from WT and KO, functional modules were specifically revealed for the KO (data deposited in <http://www.ncbi.nlm.nih.gov/geo/> under accession no. GSE68155). Interestingly, we noticed that the biological processes related to immune response, stress-activated MAPK cascade, NF- $\kappa$ B signaling, and regulation of cell death were observed among the top 20 highly significant functional modules in KO mice (Table I).

The functional modules suggested an involvement of the acquired immune system, but previous studies showed GPR34 absence leads to altered innate immune functions, such as phagocytosis (11). DCs are an important subset of the spleen cell populations (27) and they constitute the link between innate and adaptive immune responses. To inquire whether the predicted pathways are also disrupted in an isolated cell population, DCs were differentiated from mouse bone marrow cells, cultured, and subjected to RNA sequencing. The authenticity of the DC cultures

was verified by flow cytometry. DCs were investigated in the naive state and after LPS stimulation to trigger the conditions necessary to expose the immune-impaired KO mouse phenotype (6). In the naive state, 37 genes showed differential expression after multiple testing adjustments, and the only significantly overrepresented GO category between the KO and WT was related to glutamate receptor. Challenging DCs from both genotypes with LPS uncovered 155 differentially expressed genes, and 5 of the 19 enriched GO categories are involved in similar pathways to those suggested by the whole-spleen transcriptome analysis: MAPK cascade, B cell-related metabolism, TOR signaling, and phosphate metabolism (data deposited in <http://www.ncbi.nlm.nih.gov/geo/> under accession no. GSE68155).

#### GPR34 mRNA levels are reduced after TLR stimulation

Our results on DC RNA-Seq suggested that GPR34 mRNA levels are reduced after TLR4 activation through LPS (0.6-fold change,  $p = 0.06$ ). Additionally, signaling pathways predicted to be influenced by GPR34 were MAPK and NF- $\kappa$ B, which constitute the downstream activation of TLRs (28).



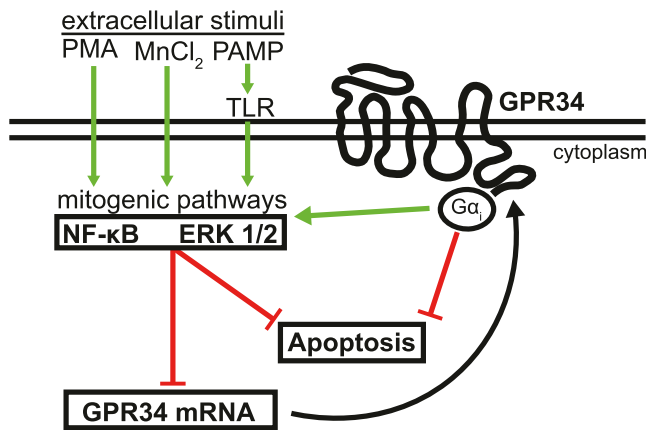


**FIGURE 7.** Graphical summary of GPR34 regulation. Stimulation of mitogenic pathways NF- $\kappa$ B and ERK1/2 leads to a decrease in the GPR34 mRNA levels. GPR34 activates ERK1/2 (38), suggesting a negative feedback mechanism (black arrow). ERK1/2 activation has an anti-apoptotic effect. Absence of GPR34 (KO) inhibits NF- $\kappa$ B and ERK1/2 phosphorylation while promoting caspase-3 activation. Caspase-3 activation stimulates apoptosis, which overall implies that GPR34 is involved in the programmed cell death mechanism.

Therefore, we inquired about GPR34 regulation after TLR stimulation. Thus, DC cultures were incubated for 8 h with TLR-stimulating compounds (details in *Materials and Methods*) and the expression level of GPR34 mRNA was indirectly measured by RT-PCR.

Tested TLR stimulants (LPS, zymosan A, R-848) led to a 20- to 30-fold reduction of the GPR34 mRNA expression (Fig. 1A). TLRs signal through both MAPK and NF- $\kappa$ B (28). To discriminate between the two pathways, GPR34 mRNA expression was quantified after preincubation with an inhibitor of NF- $\kappa$ B signaling (celastrol) and an inhibitor of MEK/ERK1/2 signaling (U0126). This resulted in a significant decrease of the effect TLR agonists have on GPR34 mRNA expression, indicating a role of both NF- $\kappa$ B and MEK/ERK1/2 in downregulating GPR34 transcription (Fig. 1B). To confirm the involvement of both TLR signaling pathways, a combination of NF- $\kappa$ B and MEK/ERK1/2 inhibitors (U0126 plus celastrol) was further tested. This hindered the reduction of GPR34 mRNA previously observed with TLR agonists (Fig. 1B). The use of both inhibitors had a significantly higher effect on reducing the mRNA decrease when compared with each of the inhibitors separately ( $p < 0.001$ ). This additive effect confirms the involvement of both NF- $\kappa$ B and MEK/ERK1/2 in reducing GPR34 mRNA expression.

To check that TLR activation does not only decrease transcription of GPR34 in isolated and differentiated DCs, experiments were also performed on mice spleens and cultured microglia. To this end, cells were incubated with LPS, a TLR4 agonist. Additionally, splenocytes were preincubated with signaling pathway inhibitors (U0126, celastrol, or both) prior to TLR4 stimulation. The expression level of GPR34 was quantified and the same tendency of signaling regulation as in DCs was observed (Fig. 2).

#### *MAPKs and NF- $\kappa$ B reduce GPR34 mRNA expression independent of TLRs*

To further address the regulation mechanism of mouse GPR34, PMA was used as a TLR-independent activator of MEK/ERK1/2 and NF- $\kappa$ B (29). The direct activation of the two pathways confirmed the results as shown with TLR agonists (Fig. 3A). The decrease of GPR34 mRNA after TLR-independent activation of MEK/ERK1/2 and NF- $\kappa$ B could also be hindered through the

inhibitors of the pathways. The combination of both inhibitors results in a complete loss of the effect that PMA has on GPR34 mRNA regulation in DCs (Fig. 3B).

Metal ions can mediate inflammatory cytokine transcription through the NF- $\kappa$ B cascade (30–32). Similarly, a decrease of GPR34 mRNA levels was shown for manganese ions, which was also hindered by preincubation with inhibitors (Fig. 3).

Thus, regardless of the nature of the upstream input, activation of MAPK (ERK1/2) and NF- $\kappa$ B signaling pathways decreases the GPR34 mRNA amount in DCs.

#### *GPR34 mRNA levels are reduced after a pulse stimulation of TLR4*

The observed reduction in the GPR34 mRNA levels could be either a direct effect of MAPK and NF- $\kappa$ B stimulation or an additive effect following continuous stimulation of the pathways. To check which of the two mechanisms is more likely, we stimulated DCs for 1 h in a pulse manner (details in *Materials and Methods*). The kinetics showed that a decrease in GPR34 mRNA expression was significant after 8 h and it remained up to 24 h ( $p < 0.01$ ) (Fig. 4). Thus, a 1-h LPS stimulation of the MAPK and NF- $\kappa$ B pathways is sufficient to trigger a prolonged decrease in GPR34 mRNA levels.

#### *GPR34 absence leads to lower ERK and I $\kappa$ B phosphorylation*

Because NF- $\kappa$ B and MAPK were functional modules affected by GPR34 absence (Table I), we tested whether these pathways are differentially activated in DCs originating from WT and KO mice. Thus, we used DCs under basal conditions and after LPS stimulation. Significantly higher phosphorylation levels of ERK1/2 and I $\kappa$ B were detected in the WT samples both under basal conditions ( $p < 0.001$  for both determinations) and after LPS stimulation ( $p_{\text{ERK1/2}} = 0.012$ ,  $p_{\text{I}\kappa\text{B}} < 0.001$ ) (Fig. 5).

#### *GPR34 absence leads to increased apoptosis in DCs*

To further follow the hypothesized GPR34-related processes, which had resulted from our transcriptome-based bioinformatics analysis (Table I), we also inquired into the influence of GPR34 absence on apoptosis. Moreover, NF- $\kappa$ B and ERK1/2, which we show to be involved in GPR34 regulation, have been previously described in apoptosis (33). To this end, DCs obtained from either WT or KO mice were cultured and stimulated with staurosporine, known to induce apoptosis (34). Caspase-3/7 activity was significantly influenced by both the genotype ( $p = 0.004$ ) and staurosporine ( $p = 0.02$ ). KO-originating DCs displayed higher caspase activity both under basal and challenging conditions (Fig. 6A).

Caspase-3 cleavage, which leads to its activation, was higher in the KO compared with the WT staurosporine-stimulated DCs ( $p < 0.001$ , Fig. 6B, 6C). Moreover, to further check caspase-3 activity, we measured the cleavage levels of PARP-1, a substrate of caspase-3. The significantly higher PARP-1 cleavage ( $p = 0.002$ ) supports a higher caspase-3 activity in the KO cells (Fig. 6B, 6C).

Furthermore, the fraction of apoptotic cells in DC cultures was measured by detecting annexin V/propidium iodide–positive cells using flow cytometry. This confirmed the significantly higher apoptosis in KO DCs after staurosporine treatment ( $p = 0.03$ ) (Fig. 6D).

## **Discussion**

GPR34 belongs to the P2Y<sub>12</sub>-like receptor group, and its expression levels have been related to impaired immunity (6, 11) and development of lymphoma and gastric cancer (35–38). Up-regulation of the receptor has also been linked to neuroinflammation (9). Thus, GPR34 mRNA expression and regulation

may be of fundamental importance for understanding the pathophysiology of these disease states, but the regulatory pathways remain unknown.

Taking advantage of a KO mouse model we identified functional modules affected by the absence of GPR34. The results revealed MAPK, NF- $\kappa$ B, and apoptosis to be impacted by the receptor deficiency (Table I), with an overlap in the transcriptomic data from both entire spleens and DC cultures (data deposited in <http://www.ncbi.nlm.nih.gov/geo/> under accession no. GSE68155).

Our previous results showed that GPR34 deficiency leads to an altered function of the innate immune system (11). The employed bioinformatics approach revealed a role in the acquired Ig-mediated immune response (Table I), which is in agreement with a previous study (6). It seems thus reasonable to assume that GPR34 could affect the function of both the innate and adaptive immune systems. DCs link the innate and adaptive immunity (39) and they express TLRs (40), which signal through both the MAPK and NF- $\kappa$ B pathways (41). Thus, to facilitate the inquiry of GPR34 regulation, the bioinformatics-revealed signaling pathways were deeper investigated in a DC culture model in the presence of TLRs stimulants. Stimulation of different TLRs leads to a reduction of GPR34 mRNA amount. This is in line with a previous profiling of GPCR expression after TLR4-mediated monocyte to macrophage differentiation, which reported an overall trend of reduced mRNA expression for the assessed GPCRs (42). We show that the decrease of GPR34 mRNA levels occurs through both MAPK and NF- $\kappa$ B pathways (Fig. 7). Moreover, the results support also a TLR-independent repression of GPR34 levels upon stimulation of either of the two pathways via other signaling routes. For the pulse kinetics of GPR34 regulation, the stimulus is removed such that ERK dephosphorylation is complete after 1 h (43). Significant reduction in the GPR34 mRNA levels occurs only 8 h after the pulse stimulation time point and is maintained up to 24 h (Fig. 4). The delayed time point of GPR34 mRNA expression decrease, as well as the persistence of the significant reduced levels for a long period, may suggest that GPR34 regulation occurs through downstream pathways activated by ERK, not by direct ERK stimulation.

Previous studies suggested that upregulation of GPR34 activates Akt and ERK (37, 38), in agreement with other findings showing that G<sub>i</sub> protein-coupled receptors activate these pathways (44) (Fig. 7). Conversely, knockdown of the receptor leads to lower ERK phosphorylation in a gastric adenocarcinoma cell line (37). Our results on DCs from WT and KO support the lower ERK phosphorylation in the absence of GPR34 in both the basal state or after stimulation with LPS (Fig. 5). ERK1/2 activation was shown to exert an antiapoptotic effect, whereas the inhibition promotes apoptosis (45) (Fig. 7). This may reflect an involvement of GPR34 in programmed cell death.

Indeed, our results support an increased apoptotic level related to the lack of the receptor. Increased caspase-3/7 activity was detected in DCs from KO mice under both basal and staurosporine-stimulated conditions (Fig. 6A). Additionally, cleaved caspase-3 and the 24-kDa cleavage product of PARP-1, a substrate of caspase-3, were present in higher levels in the KO DCs (Fig. 6B, 6C). Inhibition of caspase activity is involved in DC maturation by promoting surface expression of MHC class II (46, 47). Although morphological assessment of maturation did not show significant differences between KO and WT DCs after LPS treatment on in vitro day 10 (Supplemental Fig. 2), it cannot be excluded that the higher caspase-3 levels in the KO might lead, at another time point, to a less effective maturation of these immune cells (6).

Collectively, our study provides new insights into the mRNA regulation and reveals a role of GPR34 in the fate of DCs. We

provide a pathway that decreases the mRNA levels of the receptor. Because GPR34 overexpression could be relevant for neuro-inflammatory states (9) and cancer progression (48), the down-regulatory mechanisms described in the present study should be addressed in future studies to evaluate their therapeutic potential.

## Acknowledgments

We are especially thankful to Janet Kelso (Max Planck Institute for Evolutionary Anthropology) for helpful comments that improved the overall work. We thank Michael Dannemann, Gabriel Renaud, and Roger Mundry (Max Planck Institute for Evolutionary Anthropology) for helpful discussions regarding bioinformatics analyses and Rigo Schulz (Max Planck Institute for Evolutionary Anthropology) for excellent support of the bioinformatics infrastructure. We are grateful to Anne Butthof for great technical assistance and to Knut Krohn (Core Unit "DNA technologies," Interdisciplinary Center for Clinical Research Leipzig) and Antje Weihmann (Max Planck Institute for Evolutionary Anthropology) for performing the Illumina sequencing. We also want to thank Andreas Lösche and Kathrin Jäger (Core Unit "Fluorescence Technologies," Interdisciplinary Center for Clinical Research Leipzig) for flow cytometry analysis. We appreciate the work of Diana Chitimus, who helped improve the manuscript by performing additional gene expression experiments.

## Disclosures

The authors have no financial conflicts of interest.

## References

1. Banchereau, J., and R. M. Steinman. 1998. Dendritic cells and the control of immunity. *Nature* 392: 245–252.
2. Berchtold, S., A. L. Ogilvie, C. Bogdan, P. Mühl-Zürbes, A. Ogilvie, G. Schuler, and A. Steinkasserer. 1999. Human monocyte derived dendritic cells express functional P2X and P2Y receptors as well as ecto-nucleotidases. *FEBS Lett.* 458: 424–428.
3. Rescigno, M., C. Winzler, D. Delia, C. Mutini, M. Lutz, and P. Ricciardi-Castagnoli. 1997. Dendritic cell maturation is required for initiation of the immune response. *J. Leukoc. Biol.* 61: 415–421.
4. Schöneberg, T., A. Schulz, R. Grosse, R. Schade, P. Henklein, G. Schultz, and T. Gudermann. 1999. A novel subgroup of class I G-protein-coupled receptors. *Biochim. Biophys. Acta* 1446: 57–70.
5. Sugo, T., H. Tachimoto, T. Chikatsu, Y. Murakami, Y. Kikukawa, S. Sato, K. Kikuchi, T. Nagi, M. Harada, K. Ogi, et al. 2006. Identification of a lysophosphatidylserine receptor on mast cells. *Biochem. Biophys. Res. Commun.* 341: 1078–1087.
6. Liebscher, I., U. Müller, D. Teupser, E. Engemaier, K. M. Y. Engel, L. Ritscher, D. Thor, K. Sangkuhl, A. Ricken, A. Wurm, et al. 2011. Altered immune response in mice deficient for the G protein-coupled receptor GPR34. *J. Biol. Chem.* 286: 2101–2110.
7. Ritscher, L., E. Engemaier, C. Stäubert, I. Liebscher, P. Schmidt, T. Hermsdorf, H. Römpler, A. Schulz, and T. Schöneberg. 2012. The ligand specificity of the G-protein-coupled receptor GPR34. *Biochem. J.* 443: 841–850.
8. Sharman, J. L., H. E. Benson, A. J. Pawson, V. Lukito, C. P. Mpamhanga, V. Bombail, A. P. Davenport, J. A. Peters, M. Spedding, A. J. Harmar, and I. Nc, NC-IUPHAR. 2013. IUPHAR-DB: updated database content and new features. *Nucleic Acids Res.* 41: D1083–D1088.
9. Bédard, A., P. Tremblay, A. Chernomoretz, and L. Vallières. 2007. Identification of genes preferentially expressed by microglia and upregulated during cuprizone-induced inflammation. *Glia* 55: 777–789.
10. Engemaier, E., H. Römpler, T. Schöneberg, and A. Schulz. 2006. Genomic and supragenomic structure of the nucleotide-like G-protein-coupled receptor GPR34. *Genomics* 87: 254–264.
11. Preissler, J., A. Grosche, V. Lede, D. Le Duc, K. Krügel, V. Matyash, F. Szulzewsky, S. Kallendrusch, K. Immig, H. Kettenmann, et al. 2015. Altered microglial phagocytosis in GPR34-deficient mice. *Glia* 63: 206–215.
12. Bohnkamp, J., I. Bösel, A. Saalbach, A. Tönjes, P. Kovacs, H. Biebertmann, H. M. Manvelyan, T. Polte, D. Gasperikova, S. Lkhagvasuren, et al. 2010. Involvement of the chemokine-like receptor GPR33 in innate immunity. *Biochem. Biophys. Res. Commun.* 396: 272–277.
13. Lutz, M. B., N. Kukutsch, A. L. Ogilvie, S. Rössner, F. Koch, N. Romani, and G. Schuler. 1999. An advanced culture method for generating large quantities of highly pure dendritic cells from mouse bone marrow. *J. Immunol. Methods* 223: 77–92.
14. Renaud, G., U. Stenzel, and J. Kelso. 2014. IseeHom: adaptor trimming and merging for Illumina sequencing reads. *Nucleic Acids Res.* 42: e141.
15. Flicek, P., M. R. Amodé, D. Barrell, K. Beal, S. Brent, D. Carvalho-Silva, P. Clapham, G. Coates, S. Fairley, S. Fitzgerald, et al. 2012. Ensembl 2012. *Nucleic Acids Res.* 40: D84–D90.

16. Langmead, B., C. Trapnell, M. Pop, and S. L. Salzberg. 2009. Ultrafast and memory-efficient alignment of short DNA sequences to the human genome. *Genome Biol.* 10: R25.
17. Quinlan, A. R., and I. M. Hall. 2010. BEDTools: a flexible suite of utilities for comparing genomic features. *Bioinformatics* 26: 841–842.
18. Anders, S., and W. Huber. 2010. Differential expression analysis for sequence count data. *Genome Biol.* 11: R106.
19. Lin, C. C., J. T. Hsiang, C. Y. Wu, Y. J. Oyang, H. F. Juan, and H. C. Huang. 2010. Dynamic functional modules in co-expressed protein interaction networks of dilated cardiomyopathy. *BMC Syst. Biol.* 4: 138.
20. The Gene Ontology Consortium. 2000. Gene Ontology: tool for the unification of biology. *Nat. Genet.* 25: 25–29.
21. Prüfer, K., B. Muetzel, H. H. Do, G. Weiss, P. Khaitovich, E. Rahm, S. Pääbo, M. Lachmann, and W. Enard. 2007. FUNC: a package for detecting significant associations between gene sets and ontological annotations. *BMC Bioinformatics* 8: 41.
22. Repetto, G., A. del Peso, and J. L. Zurita. 2008. Neutral red uptake assay for the estimation of cell viability/cytotoxicity. *Nat. Protoc.* 3: 1125–1131.
23. Bolker, B. M., M. E. Brooks, C. J. Clark, S. W. Geange, J. R. Poulsen, M. H. Stevens, and J. S. White. 2009. Generalized linear mixed models: a practical guide for ecology and evolution. *Trends Ecol. Evol. (Amst.)* 24: 127–135.
24. Team, R. C. 2014. *R: A Language and Environment for Statistical Computing*. R Foundation for Statistical Computing, Vienna, Austria.
25. Bates, D., M. Mächler, B. M. Bolker, and S. Walker. 2015. Fitting linear mixed-effects models using lme4. *J. Stat. Softw.* DOI: 10.18637/jss.v067.i01.
26. Taylor, I. W., R. Linding, D. Warde-Farley, Y. Liu, C. Pesquita, D. Faria, S. Bull, T. Pawson, Q. Morris, and J. L. Wrana. 2009. Dynamic modularity in protein interaction networks predicts breast cancer outcome. *Nat. Biotechnol.* 27: 199–204.
27. Hey, Y. Y., and H. C. O'Neill. 2012. Murine spleen contains a diversity of myeloid and dendritic cells distinct in antigen presenting function. *J. Cell. Mol. Med.* 16: 2611–2619.
28. Kawai, T., and S. Akira. 2009. The roles of TLRs, RLRs and NLRs in pathogen recognition. *Int. Immunol.* 21: 317–337.
29. Chang, M. S., B. C. Chen, M. T. Yu, J. R. Sheu, T. F. Chen, and C. H. Lin. 2005. Phorbol 12-myristate 13-acetate upregulates cyclooxygenase-2 expression in human pulmonary epithelial cells via Ras, Raf-1, ERK, and NF- $\kappa$ B, but not p38 MAPK, pathways. *Cell. Signal.* 17: 299–310.
30. Felix, K., S. K. Manna, K. Wise, J. Barr, and G. T. Ramesh. 2005. Low levels of arsenite activates nuclear factor- $\kappa$ B and activator protein-1 in immortalized mesencephalic cells. *J. Biochem. Mol. Toxicol.* 19: 67–77.
31. Lewis, J. B., T. M. Randol, P. E. Lockwood, and J. C. Wataha. 2003. Effect of subtoxic concentrations of metal ions on NF $\kappa$ B activation in THP-1 human monocytes. *J. Biomed. Mater. Res. A* 64: 217–224.
32. Ramesh, G. T., D. Ghosh, and P. G. Gunasekar. 2002. Activation of early signaling transcription factor, NF- $\kappa$ B following low-level manganese exposure. *Toxicol. Lett.* 136: 151–158.
33. Becatti, M., F. Prignano, C. Fiorillo, L. Pescitelli, P. Nassi, T. Lotti, and N. Taddei. 2010. The involvement of Smac/DIABLO, p53, NF- $\kappa$ B, and MAPK pathways in apoptosis of keratinocytes from perilesional vitiligo skin: protective effects of curcumin and capsaicin. *Antioxid. Redox Signal.* 13: 1309–1321.
34. Belmokhtar, C. A., J. Hillion, and E. Ségal-Bendirdjian. 2001. Staurosporine induces apoptosis through both caspase-dependent and caspase-independent mechanisms. *Oncogene* 20: 3354–3362.
35. Ansell, S. M., T. Akasaka, E. McPhail, M. Manske, E. Braggio, T. Price-Troska, S. Ziesmer, F. Secreto, R. Fonseca, M. Gupta, et al. 2012. t(X;14)(p11;q32) in MALT lymphoma involving GPR34 reveals a role for GPR34 in tumor cell growth. *Blood* 120: 3949–3957.
36. Baens, M., J. Finalet Ferreira, T. Tousseyn, H. Urbankova, L. Michaux, L. de Leval, D. Dierickx, P. Wolter, X. Sagaert, P. Vandenberghe, et al. 2012. t(X;14)(p11;q32.33) is recurrent in marginal zone lymphoma and up-regulates GPR34. *Haematologica* 97: 184–188.
37. Jin, Z. T., K. Li, M. Li, Z. G. Ren, F. S. Wang, J. Y. Zhu, X. S. Leng, and W. D. Yu. 2015. G-protein coupled receptor 34 knockdown impairs the proliferation and migration of HGC-27 gastric cancer cells in vitro. *Chin. Med. J. (Engl.)* 128: 545–549.
38. Zuo, B., M. Li, Y. Liu, K. Li, S. Ma, M. Cui, Y. Qin, H. Zhu, X. Pan, J. Guo, et al. 2015. G-protein coupled receptor 34 activates Erk and phosphatidylinositol 3-kinase/Akt pathways and functions as alternative pathway to mediate p185Bcr-Abl-induced transformation and leukemogenesis. *Leuk. Lymphoma* 56: 2170–2181.
39. Steinman, R. M. 2006. Linking innate to adaptive immunity through dendritic cells. *Novartis Found. Symp.* 279: 101–109.
40. Reis e Sousa, C. 2004. Toll-like receptors and dendritic cells: for whom the bug tolls. *Semin. Immunol.* 16: 27–34.
41. Takeda, K., and S. Akira. 2004. TLR signaling pathways. *Semin. Immunol.* 16: 3–9.
42. Hohenhaus, D. M., K. Schaale, K. A. Le Cao, V. Seow, A. Iyer, D. P. Fairlie, and M. J. Sweet. 2013. An mRNA atlas of G protein-coupled receptor expression during primary human monocyte/macrophage differentiation and lipopolysaccharide-mediated activation identifies targetable candidate regulators of inflammation. *Immunobiology* 218: 1345–1353.
43. Zhao, Y., and Z. Y. Zhang. 2001. The mechanism of dephosphorylation of extracellular signal-regulated kinase 2 by mitogen-activated protein kinase phosphatase 3. *J. Biol. Chem.* 276: 32382–32391.
44. Gutkind, J. S. 1998. The pathways connecting G protein-coupled receptors to the nucleus through divergent mitogen-activated protein kinase cascades. *J. Biol. Chem.* 273: 1839–1842.
45. Lu, Z., and S. Xu. 2006. ERK1/2 MAP kinases in cell survival and apoptosis. *IUBMB Life* 58: 621–631.
46. Santambrogio, L., I. Potolicchio, S. P. Fessler, S. H. Wong, G. Raposo, and J. L. Strominger. 2005. Involvement of caspase-cleaved and intact adaptor protein 1 complex in endosomal remodeling in maturing dendritic cells. *Nat. Immunol.* 6: 1020–1028.
47. Wong, S. H., L. Santambrogio, and J. L. Strominger. 2004. Caspases and nitric oxide broadly regulate dendritic cell maturation and surface expression of class II MHC proteins. *Proc. Natl. Acad. Sci. USA* 101: 17783–17788.
48. Yu, W., S. Ma, L. Wang, B. Zuo, M. Li, Z. Qiao, X. Pan, Y. Liu, and J. Wang. 2013. Upregulation of GPR34 expression affects the progression and prognosis of human gastric adenocarcinoma by PI3K/PDK1/AKT pathway. *Histol. Histopathol.* 28: 1629–1638.